Canadian Science Publishing | Canadian Journal of Chemistry

Study of the Microstructure, Morphology, Micro- and Nanoindentation Hardness, and Corrosion Behavior of Ni-SiO2 Composites Electrodeposited from a Deep Eutectic Solvent

Journal:	*Canadian Journal of Chemistry*
Manuscript ID	cjc-2025-0152.R1
Manuscript Type:	Research Article
Date Submitted by the Author:	09-Oct-2025
Complete List of Authors:	Fattah, Mehry; York University - Keele Campus, Chemistry Morin, Sylvie; York University - Keele Campus, Chemistry
Is the manuscript for consideration in a Special Issue or Collection?:	ISESS 2024
Keyword:	Electrodeposition; nanocomposite; nickel; hardeness; corrosion; deep eutectic solvent

SCHOLARONE™
Manuscripts

© The Author(s) or their Institution(s)

Study of the Microstructure, Morphology, Micro- and Nanoindentation Hardness, and Corrosion Behavior of Ni-SiO_2 Composites Electrodeposited from a Deep Eutectic Solvent

Mehry Fattah[a] and Sylvie Morin[a]*

[a]Department of Chemistry, York University, 4700 Keele Street, Toronto, Ontario, Canada M3J 1P3

* corresponding author

Emails: smorin@yorku.ca

Draft

© The Author(s) or their Institution(s)

Abstract

Composite coatings containing Ni and small amounts of SiO_2 nanoparticles (NPs) were electrodeposited from an environmentally friendly deep eutectic solvent (DES) containing 0, 15, and 30 g/L of SiO_2. The effects of the presence of SiO_2 in the Ni coatings were investigated in relation to their microstructure, as well as their mechanical and corrosion properties. The average crystallite size of Ni decreased by approximately 9% with the incorporation of 30 g/L SiO_2. At this SiO_2 concentration, the Si content reached 0.56 wt.% in the bulk and 4.1 wt.% at the surface of the coating based on the results obtained by EDX and XPS, respectively. Microstructure studies of all coatings identified a granular growth with a broad Ni cluster size distribution. With the addition of 30 g/L of SiO_2, the surface roughness decreased, and the normality of the surface texture improved. Maximum micro- and nanoindentation hardness values of 4.9 $GPa_{0.0981\ N}$ (500 $Hv_{0.0981\ N}$) and 6.7 $GPa_{20\ mN}$, respectively, were achieved with the addition of 30 g/L of silica nanopowder, representing increases of 18% and 8% compared to pure Ni. Electrochemical results showed that the incorporation of 15 and 30 g/L SiO_2, along with reduced surface defects, significantly improved polarization behavior. This enhancement is attributed to improved passive film formation and the role of SiO_2 as a corrosion barrier. Corrosion current density decreased by factors of 11 and 7, respectively, compared to unreinforced Ni.

Keywords

Electrodeposition; nanocomposite; nickel; hardeness; corrosion; deep eutectic solvent

Draft

© The Author(s) or their Institution(s)

1. Introduction

Surface properties improvement processes are being sought to enhance the functionality of engineered industrial components, such as automobile and aircrafts manufacturing. Failure of the surface protection characteristics during operation lead to the low in-service efficiency and increase in projected operation cost. Therefore, this topic continues to garner serious interest, including the development of suitable hard coatings for the fabrication of industrial components with the desired hardness characteristics, that can be complex and costly. Surface properties improvement processes employ methods, such as physical vapour deposition,[1,2] chemical vapour deposition[3,4] plasma assisted treatments[5] and electrodeposition.[6-8] These methods are being implemented widely to approach this goal. Electrodeposition has been used to fabricate different surface coatings such as Ni[9,10] and Zn,[11,12] and metal matrix composites, such as Ni-TiO_2,[6,13,14] Ni-SiC,[7] Ni-SiO_2[8,15,16] and Ni-AlN[17] with the goal of improving hardness,[7,8,17] corrosion protection,[9,15,17] and their self-cleaning and wettability[6,8,10,13,17] properties. Nanomaterials addition to metal matrices attracted attention because of their high surface area to weight ratio that can be effective in modifying materials' mechanical properties, such as hardness. Electrodeposition of Ni-matrix nanocomposite coatings containing nanopaticles (NPs), such as SiC,[18] Al_2O_3,[19] SiC,[19] and SiO_2[8,20] prepared from the Watts electrolyte were investigated with the aim of improving surface hardness and corrosion properties. However, the probability of NPs agglomeration is high in this electrolyte due to the NPs high surface energy and impedes the development of coatings with the desired hardness characteristics. Deep eutectic solvents (DESs) were introduced recently by Abbott *et al*.[21] as a new environmentally friendly ionic liquid alternative and have been used since to fabricate pure metals,[22-28] alloy deposits,[29] and nanocomposite coatings[30-32] due to their superior stability with respect to moisture and air

Draft

© The Author(s) or their Institution(s)

stability,[32] dispersion[30,31] as well as being green,[32] and finally for their wide usable electrode potential window.[29-31] Li *et al.*[30,31] showed that the probability of agglomeration of NPs in Ni-SiO_2 coatings decreases by using a DES electrolyte due to the dispersion stability of DESs over that of the Watts electrolyte.

Abbot *et al*.[24] reported a maximum hardness for Ni coating electroplated from an ethaline solution containing 0.6 M of $NiCl_2{\cdot}6H_2O$ in ChCl/EG:1/2 molar ratio (choline chloride/ethylene glycol:1/2 molar ratio), in the absence of additives as equal to 389 $Hv_{0.49\ N}$ (or 3.81 GPa using 0.49 N applied load) but this value increased to 430-473 $Hv_{0.49\ N}$ (corresponding 4.22 – 4.64 GPa using 0.49 N applied load) in the presence of grain refining additives.

Abbot *et al*.[23] also compared hardness of the Ni coatings electroplated from Watts, aqueous solution (1.14 M, $NiCl_2{\cdot}6H_2O$ in water), to those prepared using ethaline (with a molar ratio of 1ChCl:2EG) containing 1.14 M, $NiCl_2{\cdot}6H_2O$. They reported a hardness of 460 $Hv_{0.49\ N}$ (or 4.51 GPa) for Ni coating electroplated from DES electrolyte, about 100 $Hv_{0.49\ N}$ (or 0.98 GPa) higher than that of the Ni coating electroplated using a Watts electrolyte. They also claimed that the DES prepared coating matches the hardness of the Ni coating electroplated from aqueous solution containing additives such as ammonium chloride (c.a. 380-480 Hv (3.73 – 4.71 GPa)) as reported by Wesley and Roehl[33] Abbot *et al*.[23] related the high hardness of the Ni coating electroplated from DES electrolyte to the growth of finer Ni grains compared to those obtained from Watts and aqueous solutions.

Danilov *et al*.[34] deposited Ni-TiO_2 coatings from DES electrolyte containing TiO_2 NPs in the absence of grain refining additives. They demonstrated that a nano-sized Ni crystallite coating was also produced. They also studied hardness behavior of their coatings as a function of the addition of NPs into the electrolyte to understand the hardness improvement mechanism. They

Draft

© The Author(s) or their Institution(s)

also concluded that a dispersion strengthening mechanism was dominant and followed the Orowan mechanism.[35]

There are reports in the literature demonstrating the advantages of using pulse electrodeposition instead of direct current for metal electrodeposition from the DES-based electrolytes[27,36] and chloride bath.[37]

Mernissi Cherigui *et al.*[27] demonstrated that applying a resting time after an electrodeposition period from a choline chloride-based DES electrolyte can decrease the probability of Ni deposition hinderance due to the passivation on the cathode surface. They explained that when the deposition at a potential of -1.1 V (versus a silver wire quasi reference electrode, Ag QRE) for 500 s was followed by a resting time of 300 s, the OH^- ions no longer were produced on the cathode surface and the OH^-/DES complexes could diffuse away from the electrode/electrolyte interface. According to these authors this phenomenon can result in the depassivation of the electrode surface.

Rosoiu *et al*.[36] compared Ni-Sn alloy electrodeposited from a choline chloride/ethylene glycol eutectic mixture DES electrolyte using pulse and direct current. They demonstrated that by using pulse current electrodeposition, the crystallite size of the coating decreased and better hardness results were obtained.

Ashassi-Sorkhabi *et al.*[37] compared the electrodeposition of Ni-Zn alloy by using direct and pulse current from an aqueous-based chloride electrolyte and showed that pulse current decreased the precipitation of the zinc hydroxide on the cathode surface and resulted in the improved electrodeposition current efficiency.

Additionally, it has been shown that the pulse current electrodeposition has some advantages over DC current for composite coatings electrodeposition such as: increased particle content in

© The Author(s) or their Institution(s)

the coatings,[38] finer grain size with improved hardness,[38,39] improved wear resistance,[38,40] and better corrosion resistance and more uniform surface, due to the effect of the resting time through the off time of the pulse current.[39,40]

It has been demonstrated by Yang and Cheng[41] that a decrease of duty cycle from 80 to 20% at fixed frequency increased the amount of SiC NPs embedded in the coating led to an increase in the hardness and corrosion resistance of the Ni-Co-SiC nanocomposite coating. They obtained a Ni-Co-SiC nanocomposite coating with a higher number of deposited NPs in the coating, improved hardness and corrosion resistance by using a higher frequency and lower duty cycle.

Jiang *et al*.[42] evaluated the effect of the frequency of the pulse current on the growth mechanism and morphology of the surface electrodeposited from an electrolyte containing lanthanum chloride (0.04 M), myristic acid (0.1 M), and ethanol (150 ml), on Cu surface at an electrodeposition voltage of 30 V, a 50% duty cycle, ambient temperature and stirring rate of 200 rpm for 10 min. Based on their results, frequency is identified as the critical parameter that can define the final morphology of the coating, by affecting the crystal nucleation and growth rate. These authors also reported that the rate of nucleation and growth at a frequency of 1000 Hz resulted in an homogeneous distribution of particles, and a micro/nano hierarchical structure that further increased the superhydrophobicity of the surface. They also confirmed the presence of cracks on the surface when frequencies higher than 1000 Hz were used.

Li *et al.*[43] reported that for the electrodeposition of Ni-W/B_4C an increase of the pulse frequencies from 1 to 1000 Hz, resulted in a decreased in grain size, an increase in NPs content, and the formation of a smoother coating surface. In addition, the microhardness of the coating increased to the maximum amount when a frequency of 1000 Hz was employed.

© The Author(s) or their Institution(s)

Although several studies[30-32,34] have reported the fabrication and characteristics of nanostructured Ni-matrix nanocomposites electroplated from DES-based electrolyte containing NPs, the relationship between the electrodeposition conditions and the coating properties as well as the origin of the strengthening mechanism require more investigations. Fattah and Morin have investigated the effect of the pulse current density with a frequency of 1000 Hz, and duty cycle of 27%, on the hardness and corrosion properties of the Ni coatings electroplated from a DES-based electrolyte.[44] That work established that the effective range of electrodeposition current densities necessary to fabricate Ni coatings with improved corrosion protection properties while enhancing microindentation hardness was between 1 and 8 mA cm^{-2}. The maximum current efficiency for the electrodeposition of a crack free coating was obtained for the Ni coating electroplated at 8 mA cm^{-2} with no evidence of pitting corrosion after potentiodynamic polarization experiment, while the relation between hardness and Ni crystallite grain size was consistent with the inverse Hall-Petch relationship.[44]

Based on the current knowledge, the objective of this paper is to use an environmentally friendly deep eutectic solution as a green approach to produce high performance coatings with further improved hardness and corrosion properties compared to Ni coatings prepared in aqueous electrolytes. Another approach to modify coatings properties is through the addition of SiO_2 NPs. In this study SiO_2 concentrations of 15 and 30 g/L were added to the ethaline-based DES electrolyte to fabricate Ni-SiO_2 nanocomposite coatings. This article focuses on the effects of the NP incorporation in the Ni matrix, on the coating's characteristics such as microstructure and morphology, composition, surface texture, and consequently on the hardness and corrosion performances of the Ni-SiO_2 electrodeposited coatings. The results will be compared to those of the Ni coating prepared from the same electrolyte in the absence of SiO_2 as well as with reports

Draft

© The Author(s) or their Institution(s)

from the literature.[44] Several characterization methods were employed to study the microstructural and compositional properties of the composites, such as scanning electron microscopy (SEM/EDX), optical microscopy, X-ray diffraction (XRD), X-ray photoelectron spectroscopy (XPS), and surface texture characterization. Surface hardness and strengthening behavior upon the addition of SiO_2 were investigated, using micro- and nanoindentation hardness measurements. While, the corrosion properties of the coatings were studied by using polarization potentiodynamic experiments. Hardness measurements and polarization experiments were performed on the composite coatings electroplated from the ethaline-based DES electrolyte containing 15 and 30 g/L of SiO_2 NPs. Then studied and compared with the results obtained from the Ni coating electroplated from the electrolyte in the absence of NPs.

A Supplementary Materials document that includes additional information and figures is also provided (references to this material are denoted with the prefix S).

2. Materials and methods

2.1. Materials and preparation. Disc shaped AISI 1045 (CK45) medium carbon steel (0.45 wt.% carbon, Metal Supermarkets) with a diameter of 19 mm and thickness of 7 mm was used as the substrate. Samples were ground and polished to a mirror finish, then degreased and activated using 0.75 M NaOH and 1.87 M H_2SO_4 as explained precisely in section S1.1, Supplementary Materials. Silica NPs from Sigma Aldrich 5-20 nm in diameter and ≥ 99.5% purity was used as purchased. Choline chloride (ChCl, $C_5H_{14}ClNO$) ≥ 98.0% purity from Alfa Aesar and ethylene glycol (EG, $C_2H_6O_2$), ≥ 99.0% purity from Fisher Bioreagents were used as purchased to prepare the DES mixture. A solid Ni plate (99.9 wt.% purity) was used as the anode for all electrodeposition experiments.

Draft

© The Author(s) or their Institution(s)

2.2. Electrodeposition. The choline chloride (ChCl)/ethylene glycol (EG)-based DES was used as the electrolyte for the electrodeposition of the composites. Choline chloride and ethylene glycol were mixed with a 1:2 molar ratio (also called ethaline) at a temperature of 70 ± 2 °C and stirred at 500 rpm ± 5% stirring rate until a colorless and clear solution was obtained. Then solid $NiCl_2{\cdot}6H_2O$ was added to the prepared ethaline solution to achieved a 0.2 M concentration of $NiCl_2{\cdot}6H_2O$. The electrolyte was prepared on the basis of the procedure reported by Abbott *et al.,*[45,46] and explained in detail for Ni electrodeposition in the previous work.[44] For the electrodeposition of Ni-SiO_2 nanocomposite coatings, 15 or 30 g/L silica NPs were added to the solution. Nanopowder weighing was done using a balance with the readability of 0.1 mg. Details regarding the procedure used to add SiO_2 to the DES electrolyte as well as images of DES (ethaline) electrolytes containing 0 and 15 g/L of SiO_2 NPs are shown in Figure S1 can be found in the Supplementary Materials section S1.2. The quality of the electrolytes were monitored using pH and conductivity up to one month after the electrolyte were prepared. The procedure and method employed, background information and results related to the DES stability are presented in section S1.2 and S2.1. Overall, the DES solutions with and without SiO_2 NPs were found to be very stable. The electrodeposition process was carried out under the same conditions for all composite coatings as shown in Table 1. Electrodeposition process was performed for 90 and 180 min, the latter yielded a total charge (i.t) of ≈ 900 C, that was necessary to prepare composite coatings with high enough thicknesses (ca. 25 μm) for microindentation hardness measurements on the cross-section and surface of the coatings in accordance with ASTM E384-17 (see section 2.4). A Dynatronix Dp20-5-10, pulse power supply with the average output current and voltage of 0-5 A and 0-20 V, respectively, was used to provide square wave pulse currents for electroplating. The average current was set and

Draft

© The Author(s) or their Institution(s)

controlled using a Fluke digital multimeter with a resolution of 0.01 mA and 0.1 mV. The square wave, frequency and duty cycle of the pulse current was confirmed by using a Tektronix digital oscilloscope.

Table 1. Ni and Ni-SiO_2 coatings electrodeposition conditions

Electrodeposition Parameter	Values
Current density ± 0.2 (mA cm^{-2})	8.0
SiO_2 concentration ± 0.5 (g/L)	0.0, 15.0 and 30.0
Frequency ± 10 (Hz)	1000
Duty cycle ± 0.2 (%)	27.0
Temperature ± 2 (°C)	70
Stirring rate (rpm) ± 5%	1000
Time ± 1 (min)	90, 180

2.3. Microstructural and compositional study. Cross-sections of the composite coatings were prepared by cutting, grinding and polishing the samples to obtain a smooth cross-section for microstructural study (see S1.3 in Supplementary Materials). The microstructure and morphology of the coatings were studied using scanning electron microscopy (Quanta 3D SEM, EDX, Imaging Facility at York University, Toronto), and optical microscopy (Olympus). Surface texture measurements, topography and histograms of the composite coating surfaces were performed employing Alicona Infinite Focus G5 3D surface measurement system (McMaster University, Hamilton, ON). All surface roughness measurements were done under ISO standards 4287 and 25178 on a 1.62 mm × 1.62 mm area.

The composite coating structure and phase analysis was performed using a Bruker D8 DISCOVER (Analytical X-Ray Diffraction Facility, McMaster University, Hamilton, ON) with a Co target with 1° incident angle and at a rating of 30 KV and 20 mA. XRD patterns were

© The Author(s) or their Institution(s)

acquired using 0.02° step increments for 3 s in the range of 2θ = 40 - 120°. A pattern search/match was executed for Ni using the ICDD PDF-4+ 2021 powder database integrated in the DIFFRAC.EVA software (version 5.2).

The XPS analysis was performed employing a PHI Quantera II, Physical Electronics, instrument (Biointerfaces Institute, McMaster University, Hamilton) using monochromatic Al K-α source. X-ray setting was defined by the manufacturer and was set at the power of 50 W and voltage of 15 KV for the area of 200 μm^2 (circle). The instrument base pressure was 1.33×10^{-7} Pa. High resolution spectrum for Si 2p was obtained from an area of 200 μm^2 (circle), with pass energy of 26, 55 and 26 eV, respectively. The step size was 0.1 eV for all the elements measured. The obtained spectrum was analyzed using CasaXPS software version 2.3.20 rev.1.2H.[47] The spectrum peaks were charge corrected to the signal of C 1s utilizing the binding energy of adventitious carbon, 284.8 ± 0.2 eV, and a Shirley background was used for the peak fitting with offset specified to achieve the best fit with the minimum standard deviation. The line shape of Gaussian (70%) – Lorentzian (30%), defined as GL(30) in CasaXPS, was used to define the shape of the Si peak. Sputter cleaning was performed using Ar^+ beam for 10 s on the sample surface and XPS spectrum was recorded before and after sputter cleaning to distinguish the components that appeared on the surface due to the exposure to the atmosphere (as the sample was kept in air for several weeks before XPS experiments were done) from compositions created during electrodeposition. Obtained fits were used to extract quantitative information from the spectrum.

2.4. Micro- and nanoindentation hardness measurements. All micro- and nanoindentation hardness measurements were done on both surfaces and cross-sections of the composite coatings. According to ASTM E384-17, to eliminate the effect of the substrate hardness and

Draft

© The Author(s) or their Institution(s)

coating layer edges on the coating's microindentation hardness values, the thickness of the coatings must be more than 10 times of the indentation depth[48] and thick enough to provide appropriate distance between the center of the indentation and the edges of the coating cross-section (at least 2.5 times the Vickers diagonal based on ASTM E384-17). Therefore, the total Ni and nanocomposite coating electrodeposition charge, for the samples used for micro- and nanoindentation hardness measurements, was set to produce coatings with 25 μm thicknesses (see section 2.2).

Cross-sections of the coatings were prepared according to the process explained in section 2.3 and additional information is provided in section S1.3 (see Supplementary Materials). The Ni coating and composite surfaces were gently polished using Struers MD-Nap cloth and DiaPro Nap B 1 μm suspension, before micro- and nanoindentation measurements on the surface. The polishing was minimal to prevent the coatings from becoming too thin (based on ASTM E384-17) to avoid any influence of the substrate hardness on the results.

Microindentation hardness measurements values were measured employing a digital micro-Vickers hardness tester, MET-MHV1k connected to a Clemex CMT.HD intelligent microscopy for image analysis (Lassonde school of Engineering, York University, Toronto, ON) using a Vickers square-based pyramid diamond indenter with the angle of 136° between the opposite faces at the vertex, applying 10 gf (0.098 N) and 50 gf (0.49 N) load for cross section and surface of the coatings, respectively.

Anton Paar nanoindentation tester (Material Property Assessment Laboratory (MPAL), McMaster University, Hamilton, ON) was employed to perform nanoindentation hardness measurements by using a Berkovich diamond type indenter tip with a face angle of 65.3 ± 0.3°. A maximum load of 20 mN was applied with loading and unloading rate of 40 mN min^{-1} and

Draft

© The Author(s) or their Institution(s)

peak load hold time of 5 s. Results were analysed based on Oliver and Pharr calculation approach.[49] The presented hardness values are the average of at least 10 hardness measurements for each sample.

2.5. Electrochemical measurements

Potentiodynamic polarization experiments were carried out using a VoltaLab 80 PGZ402 universal potentiostat analyzer. The Teflon electrochemical cell (see Fig. S11) contained three electrodes, the sample as a working electrode, a saturated calomel reference electrode (SCE), and a platinum coil as counter electrode. The working electrode area exposed to the electrolyte was the same for all samples and equal to 0.91 cm^2. All Experiments were performed in 0.6 M NaCl aqueous solution at room temperature (22 ± 2 °C). Potentiodynamic polarization curves were done at a scan rate of 2 mV s^{-1}, and corrosion parameters were analyzed and determined using a VoltaMaster 4 software based on the Tafel extrapolation method and Stern-Geary theory. All samples were immersed in a 0.6 M NaCl aqueous solution until the open circuit potential (E_{OCP}) remained unchanged (about 30 min) before potentiodynamic polarization experiments were done. In our study E_{corr} and E_{ocp} values are equal for all samples. Because the cathodic branches are too short and the anodic branches do not exhibit clear linear regions for some samples (due to the scan rate of 2 mV s^{-1}), different approaches were used to obtain corrosion current density and polarization resistance. Polarization resistance was obtained using linear polarization resistance/Stern-Geary by linear fitting in the ± 10 mV range around E_{corr} with regression coefficients $R^2 \geq 0.99$, as well as using EIS experiment results where R_p was obtained for selected samples. Cathodic and anodic slopes (β_c and β_a, respectively) were determined by extrapolation of linear portion of polarization curve within ± 150 mV around E_{corr}. A segment of 50 mV within 50 - 150 mV away from E_{corr} was selected for linear fitting, ensuring

Draft

© The Author(s) or their Institution(s)

a regression coefficient of $R^2 \geq 0.98$ (typically ≥ 0.99). Finally, average values of corrosion current densities and polarization resistances, including those obtained from the Tafel fitting using VoltaMaster 4, were reported with uncertainties expressed as deviations. All potentiodynamic polarization experiments were done for at least three samples for each individual condition. Average values were obtained and the data the closest to the average values are reported in the graphs.

3. Results and discussion

3.1. Current efficiency

The current efficiency for the electrodeposition condition chosen (see Table 1) was calculated using equation S1[24] and the measured coating mass ($\Delta m_{measured}$) and theoretical mass ($\Delta m_{theoritical}$), according to the procedure explained in detail in ref. 44. $\Delta m_{theoritical}$ is calculated using Faraday's law (see section S2.2 Supplementary Materials for more details).

The current efficiency for the electrodeposition of Ni from ethaline solution containing 0.2 M $NiCl_2{\cdot}6H_2O$ at current density of 8 mA cm^{-2} was obtained equal to 89.0 ± 0.5%.[44]

The current efficiency for Ni electrodeposition from the electrolyte containing SiO_2 NPs was obtained based on the work done by Rudnik *et al*.[50] by applying a factor of (1 – (SiO_2 wt.%)) for $\Delta m_{measured}$ in equations S1. The weight percentage of embedded SiO_2 NPs in the Ni matrix (SiO_2 wt.%) was in the range of 0.56 to 4.10 wt.% based on the results obtained through EDX and XPS measurements, respectively (see sections S2.4 and 3.3). The results also showed that the current efficiency decreased from 89 to 84 and then 81 wt.% with the addition of 0, 15 and 30 g/L of SiO_2 NPs into the electrolyte, respectively.

This reduction of current efficiency can be related to the interference of the particles movement at the substrate/electrolyte interface with the charge transfer mechanism taking place during the

Draft

© The Author(s) or their Institution(s)

Ni electrodeposition process. The decrease of current efficiency with the addition of NPs into the electrolyte was first explained by Webb and Robertson,[51] and observed and supported by others.[19,52,53]

3.2. X-ray diffraction pattern. XRD pattern for the SiO_2 NPs employed in this study is shown in Figure S3 (section S2.3, Supplementary Materials). The results demonstrate a weak crystalline structure for the SiO_2 NPs. XRD results for Ni and Ni - SiO_2 nanocomposite coatings electroplated from the electrolyte containing 15 and 30 g/L of SiO_2 NPs are displayed in Figure 1. A face-centered cubic (fcc) Ni structure with identical crystallographic planes at 2θ = 52.3°, 61.0°, 91.8° and 115.1° related to the (111), (200), (220) and (311) planes, respectively, are observed for all samples. Very weak peaks related to the Fe-α phase of the AISI 1045 medium carbon steel substrate were observed at 2θ = 52.3°, 77.4° and 99.6° and corresponded to the (110), (200) and (211) planes, respectively. The peaks corresponding to the SiO_2 NPs are not resolved in these XRD patterns due to the small concentration of embedded NPs in the Ni matrix and the amorphous nature of this material.

Texture coefficient (TC) and the standard deviation (σ) of each (h k l) crystallographic plane observed in the XRD pattern are calculated according to method reported by Gao, *et al.*,[54] and plotted as a function of the SiO_2 concentration in the electrolyte (see Figure S4, explained in section S2.3). In this work, the texture coefficients for the coatings electrodeposited from electrolytes containing 0 and 15 g/L SiO_2 NPs (Figure S4) show a minor preferred orientation for the (111) plane, that changes and favors the (220) plane with an increase in the SiO_2 concentration to 30 g/L. An acceptable standard deviation (σ = 0.2, Figure S4) was obtained for all coatings that support the absence of a strong texture in the coatings prepared with and without SiO_2 NPs.

Draft

© The Author(s) or their Institution(s)

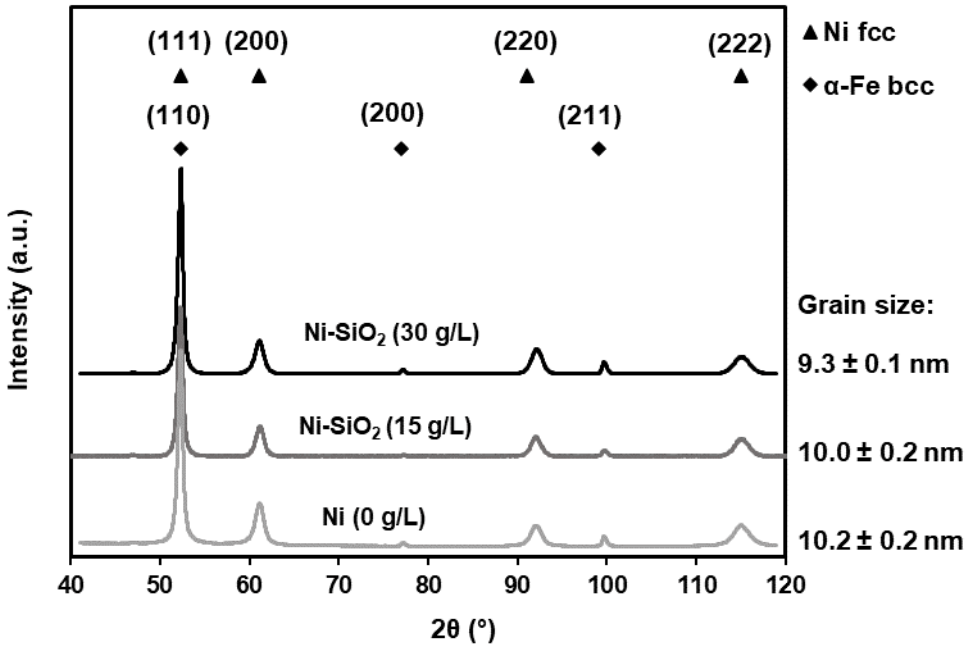

Figure 1. X-ray diffraction pattern for Ni and Ni-SiO_2 nanocomposite coatings electroplated at 8 mA cm^{-2} for 90 min from an electrolyte containing 0, 15 and 30 g/L SiO_2 NPs.

Ni average crystallite size was calculated using the Debye-Scherrer equation[55] (equation S6, section S2.3) and XRD pattern information. Because the peak at 2θ = 52.3° is a common peak for Ni and Fe, the contribution of Ni fcc was obtained from the quantification of XRD pattern at 2θ = 52.3°, the width of the peak at half height was then used to calculate the Ni crystallite sizes and texture coefficients.

Nickel grain size is in the nanometer range (10.2 ± 0.2 nm) for the coating electroplated in the absence of NPs (Figure 1), which is small compared to the sizes obtained when Watts electrolytes were employed.[19,56-58] Bhardwaj *et al.*[58] studied the grain size refining for Ni electrodeposition from a Watts bath with the addition of different amounts of additives and using applied current pulses of up to 1.5 A cm^{-2}. The smallest Ni grain size obtained for their Ni

© The Author(s) or their Institution(s)

coating was 22 nm.[58] Upon addition of 30 g/L SiO_2 NPs to the electrolyte a small decrease in the Ni average crystallite size from 10.2 ± 0.2 for the Ni coating, to 9.3 ± 0.1 nm for the Ni-SiO_2 coating was observed (see Figure 1).

3.3. Ni-SiO_2 composite composition. The effects of the presence of SiO_2 on the chemical composition of the coatings was investigated employing EDX and XPS, respectively. For these experiments the properties of the Ni-SiO_2 coatings electroplated from electrolyte containing 30 g/L of SiO_2 are compared to those prepared using the SiO_2-free electrolyte. The results obtained from EDX are shown in Figure S5, section S2.4. The EDX spectrum of the Ni coating was also studied to make sure that the amount of Si detected on the surface of the nanocomposite is only related to the incorporation of SiO_2 into the Ni matrix, and no Si was detected in the pure Ni coating.

Nickel, oxygen, and silicon with elemental atomic percentages of 93.8, 5.67 and 0.53 at.% (SiO_2, 1.6 at.%, 0.56 wt.%), respectively, were detected in the nanocomposite coating electroplated from electrolyte containing 30 g/L of SiO_2 NPs. The weight percentages of SiO_2 were 0.32 and 0.56 wt.% in the coating when 15 and 30 g/L SiO_2 NPs were present in the electrolyte. The presence of carbon and oxygen peaks in the EDX spectra are common and they have been observed for Ni coatings electroplated from various electrolytes, including Ni Watts bath and aqueous solutions.[59] The presence of Si was also detected at the surface of the Ni-SiO_2 coatings electroplated from electrolyte containing 30 g/L of SiO_2 NPs by employing XPS (see Figure 2). The XPS spectrum obtained for the pure Ni coating is also provided in Figure 2 for comparison.

Draft

© The Author(s) or their Institution(s)

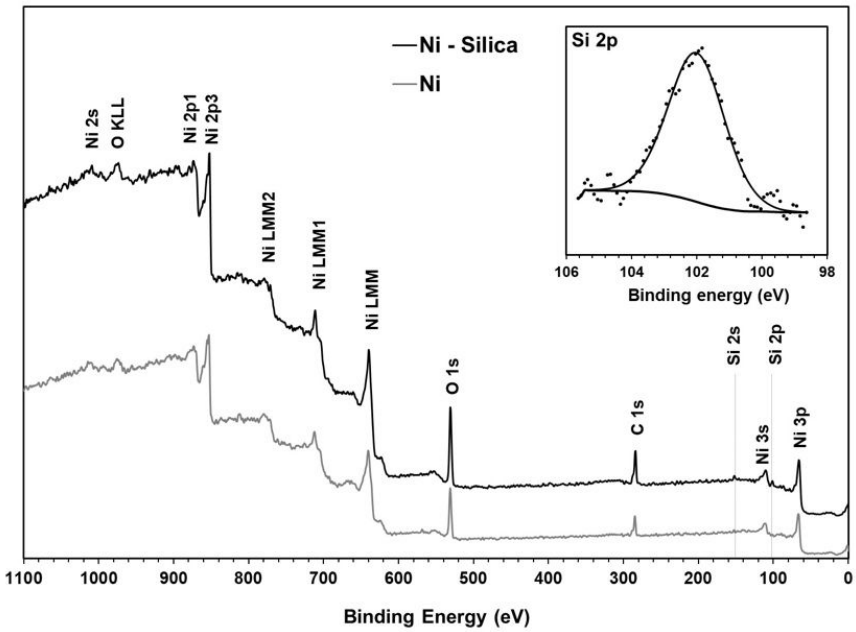

372

373 **Figure 2.** XPS survey spectra obtained for a Ni-SiO_2 nanocomposite electroplated from an
374 electrolyte containing 30 g/L (black line) and 0 g/L SiO_2. (gray line). Small peaks can be
375 observed in the Ni-SiO_2 composite that correspond to Si at 102 and 148 eV corresponding to Si
376 2p and Si 2s, respectively. High resolution Si 2p spectrum after sputter cleaning, taken from the
377 surface of Ni-SiO_2 composite electroplated from electrolyte containing 30 g/L SiO_2 is also
378 shown (insert).

379 The presence of embedded silicon in the Ni-SiO_2 coating was detected in the spectrum collected
380 from the surface of the Ni-SiO_2 coating and confirmed when compared with the spectrum
381 obtained from the surface of the SiO_2-free Ni coating (Figure 2). The peak fitting for the Ni-
382 SiO_2 coating spectrum revealed peaks corresponding to Si 2p and Si 2s at binding energies of
383 102 and 148 eV that are not detected in the SiO_2-free sample. High resolution spectrum of Si 2p
384 at the binding energy of 102.1 eV collected form Ni-SiO_2 coating surface after sputtering is also
385 shown in Figure 2 insert. XPS experiments were performed on three different locations at the
386 surface and the average amounts of the Si atomic concentration acquired from the coating

© The Author(s) or their Institution(s)

surface is reported as the Si atomic concentration. The atomic concentration of Si at the Ni-SiO_2 coating surface was 1.5 at.% and increased to 2.6 at.% (SiO_2, 4.1 wt.%) after Ar^+ sputtering. This increase is related to the remove of oxygen and carbon components from the surface through an Ar^+ sputtering pre-treatment. When only considering the Ni and Si atomic percentages in the as prepared and after sputter cleaning of the coating was performed, the ratio of the atomic percentages of Si and Ni is equal to 0.05 and it is identical for both surface preparation conditions indicating that the Si content in the coating is uniform (see Section S2.4).

With such low percentages of SiO_2 in the coatings it is not surprising to see differences between the values obtained from EDX and XPS as these two techniques do not sample the same area and depth of the sample. The amount obtained is also comparable with SiO_2 content in the Ni matrix that were electroplated from different electrolytes.[15,60]

3.4. Ni composite morphology. SEM images of Ni and Ni-SiO_2 composite coatings are shown in Figure 3. SEM image of the NPs are also provided in Figure S7. The SiO_2 NPs are spherical in shape and have diameters ≤ 50 nm. Study of the images (Figure 3) at the magnifications of 3,500× and 8,000×, shows a granular-like microstructure for all Ni and Ni-SiO_2 nanocomposite coatings.

Draft

© The Author(s) or their Institution(s)

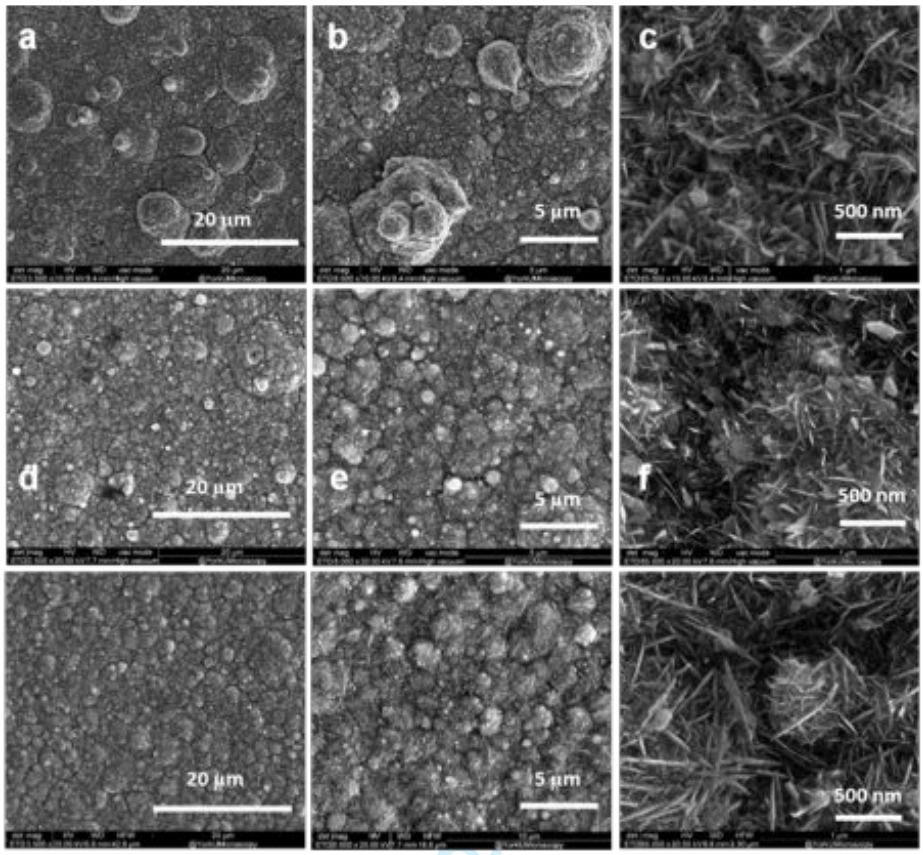

Figure 3. SEM micrographs of the coatings surface morphology for a, b, and c) SiO_2-free Ni coating, and Ni-SiO_2 nanocomposite coatings electroplated from electrolyte containing d, e, and f) 15 g/L, and g), h), and i) 30 g/L SiO_2. All coatings are electrodeposited at 8 mA cm^{-2}. The magnifications for micrographs a) d) and g); b), e) and h); and c), f) and i) are 3,500 ×, 8,000 × and 65,000 ×, respectively.

At these magnifications, Ni grains have similar growth pattern that produce a cauliflower-like appearance. The addition of SiO_2 NPs into the electrolyte didn't influence the morphology of coatings but affected the size of the cauliflower-like structure remarkably. With the addition of 15 g/L of NPs into the electrolyte, these features decreased significantly in size and doubling the concentration of NPs to 30 g/L produced no significant further changes in size of these

© The Author(s) or their Institution(s)

features. Further magnification (65,000×), reveal an interesting morphology consisting of thin features (platelets) oriented on their edges with respect to the surface plane, revealing the presence both micro- and nano-structural features at the coating's surface.

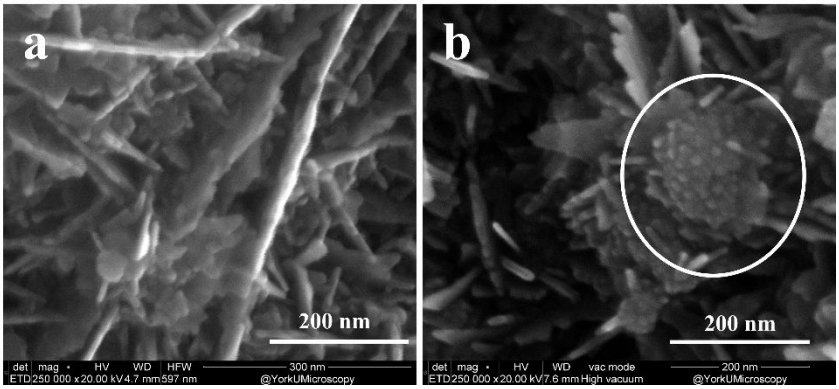

Figure 4. SEM micrographs of the surface of the coatings electroplated at 8 mA cm^{-2} from DES electrolyte containing a) 0 and b) 15 g/L SiO_2 NPs at 250,000× magnification. Smaller clusters are visible within the white circle and beyond in b).

The appearance of these platelets was not greatly influenced by the addition of NPs to the electrolyte (Figures 3 c), f) and i)). With further magnification to 250,000×, fine clusters, about 200 nm in size, consist of nanosized features are clearly distinguishable (Figure 4 b, see cluster within the circled area). It is also possible to make out some of these fine features in Figures 3 c), f) and i), hence they are not arising from the addition of SiO_2 NPs.

Figure 5 shows SEM side-view images of the Ni and Ni-SiO_2 coatings, the latter was electroplated from the electrolyte containing 15 g/L SiO_2. A columnar microstructure, composed of numerous smaller clusters, forming the layer can be identified. These columnar features start at the first stage of the electrodeposition and continue throughout growth process. A close inspection of the SEM images shown in Figures 3 b), e) and h) allow the identification

Draft

© The Author(s) or their Institution(s)

of the grain boundaries between these columns (these grain boundaries are also seen in Figure 5 b) and c). The diameter of these columnar features decreases in diameter, on average, with the addition of SiO_2 in the coating. Similar features have been observed for deposition of Ni from DES in the absence of SiO_2, these micron and nanometer features displayed the lotus effect due to having this nano and micron length-scale feature combination.[22]

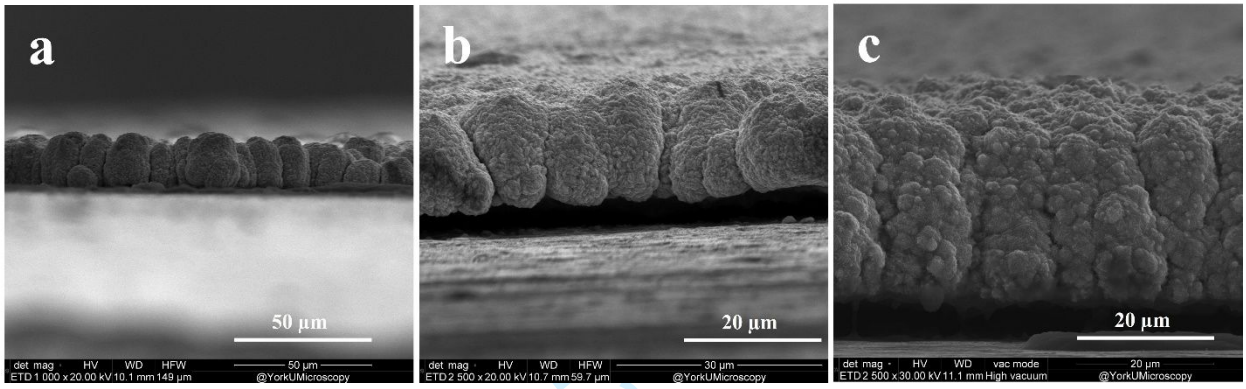

Figure 5. SEM micrographs of the profile of the coatings electroplated from DES electrolyte containing a) 0 g/L SiO_2 NPs and 1000× magnification, b) 0 g/L SiO_2 NPs and 2500× magnification, and c) 15 g/L SiO_2 NPs and 2500× magnification. Note that a) the apparent separation between the coating layer and the substrate can be related to the presence of the tape, as it was not detected through cross-section analysis; and b) these images were acquired with the film edge position at different distances and angles (not perfectly perpendicular). Hence, they cannot be used for quantitative coating thickness analysis.

The thickness of the coatings was measured using optical microscopy images taken from the cross-section of the samples, before and after etching. Figure S8 shows the quality of the cross-section of the coatings prepared before the etching step (see section S2.5). Figure 6 shows the cross-section optical microscopy images of the coatings after etching. Coating thicknesses of

© The Author(s) or their Institution(s)

13.7 ± 0.8, 12.8 ± 1, and 11.8 ± 0.4 µm were measured for Ni coating and Ni-SiO_2 coatings electroplated from electrolyte containing 0 g/L, 15 g/L, and 30 g/L SiO_2, respectively. The slight decrease of the thickness with the addition of 30 g/L SiO_2 to the electrolyte is compatible with the results obtained for the current efficiency in section 3.1. Figure 6 also highlight the uniformity of all coating layers. The intact interface between layer and substrate after cutting and metallographic processing also indicates a satisfactory adherence of the coating to the substrate (Figures 6 and S8 in section S2.5).

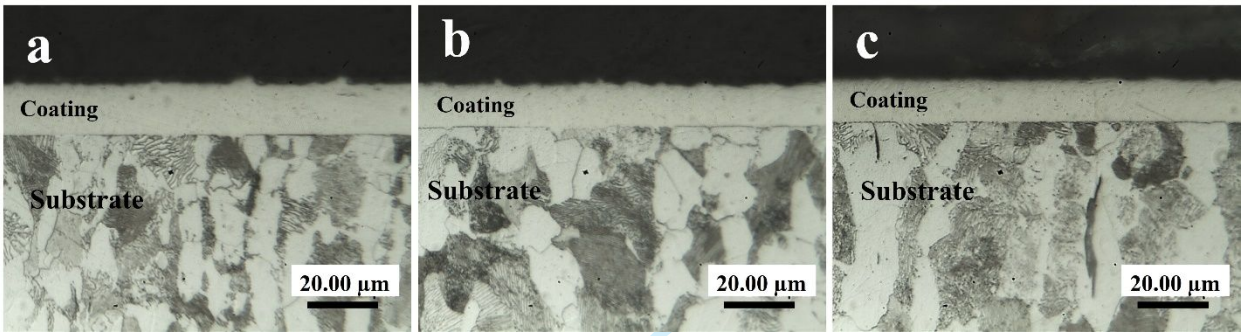

Figure 6. Cross-section optical microscopy images for coatings electroplated from electrolyte containing a) 0 g/L, b) 15 g/L, and c) 30 g/L SiO_2.

Considering all topography results, the addition of SiO_2 NPs to the DES electrolyte (for the conditions employed in this work) results in a decrease in the coating surface roughness and number of irregularities, and a more normal and symmetrical height distribution.

This phenomenon as well as the effect of the addition of SiO_2 NPs on the Ni nucleation, grain, and cluster growth during electrodeposition can be explained by considering the nucleation and growth mechanism reported for Ag deposition from a DES (ethaline-based) electrolyte proposed by Abott *et al.*[61] These authors described a 3D hemispherical nuclei formation on the substrate through electrodeposition that led to the formation of large clusters because of the

© The Author(s) or their Institution(s)

coalescence of the initial formed nuclei. A depletion zone develops around theses clusters that prevents new nucleation, while adatoms are being adsorbed on the growing clusters. They explained that it is the coalescence of those growing clusters that give rise to the observed film morphology. They also proposed two kinetics regimes in their system: isolated island growth at the very first stage of deposition and coupled growth that takes place once islands are covering the surface. In the former, the growth of isolated islands takes place with lateral and vertical growth being independent of each other, however for the coupled growth, vertical rather than lateral growth is larger due to the impingement of the growing islands.[61] Ustarroz *et al.*[62] proposed the so called electrochemical aggregative growth mechanism that supports the formation of nanostructures during electrodeposition where small, stable nanoclusters form first, then aggregate due to surface tension and coalesce into larger, sometimes defect-containing monocrystalline particles. They demonstrated that their proposed mechanism is significant and that it explains how the electrodeposition steps, such as nanocluster self-limiting growth, surface diffusion, aggregation and coalescence, can be controlled to produce specific nanometre and micrometer scale morphology and improved properties. Self-limiting growth ensures the growth of the primary nanoclusters a few nm in sizes, depending on the electrodeposited material chosen. The overall morphology of the deposit depends on the balance between nucleation and the nanocluster surface diffusion that are both dependent on overpotential.[62] This mechanism is also observed for electrodepostion from DES.[26,27] The typical morphology of the aggregative growth mechanism, is also observed for our Ni coating on steel substrates in the absence[22,44] and presence of SiO_2 NPs (this work) indicating that the electrodeposition mechanism is similar when galvanostatic deposition is used. The morphology

Draft

© The Author(s) or their Institution(s)

arising from the islands lateral and vertical growth are visible in the SEM micrographs shown in Figure 5, which supports the formation of microscopic columnar features.

3.5. Ni-SiO_2 composite hardness.

Micro- and nanoindentation tests were conducted to evaluate hardness properties of the coatings. Ni-SiO_2 nanocomposites consist of two distinct phases, Ni matrix and SiO_2 NPs. Detected amount of SiO_2 in the film is 0.56 and 4.1 wt.% based on EDX and XPS experiments, respectively (as explained in section 3.3). We are assuming that these are evenly distributed in the Ni deposit. However, there could be some accumulation of SiO_2 at the grain boundaries but not in a significant amount since silicon was not detected by XRD or using EDX mapping (Figure 1 in section 3.2. and Figure S6 in section S2.4., in Supplementary Materials). However nanoindentation results can vary depending on whether the indenter contacts the Ni phase, particle location, or phase interfacial region. To minimize this variability, all nanoindentation values were averaged from at least 10 to 15 indentations, with indents spaced sufficiently large to avoid overlap or interaction effects (≥ 5× the diagonal length of the indent, based on ASTM E2546-15) as shown in Figure 8 B. Importantly, microindentation tests, which probe a significantly larger volume than nanoindentation and thus average out local heterogeneities, revealed the same trend in hardness enhancement (see Figures 7 and 8). This consistency across both scales confirms that the observed increase in hardness is a bulk material response, attributable to the incorporation of SiO_2 NPs and not a measurement artifact. Nevertheless, some degree of scatter is inherent to such measurements and is reflected in the standard deviation.

Micro- and nanoindentation hardness measurements are displayed as a bar graph in Figures 7 and 8 and discussed in the following sections.

Draft

© The Author(s) or their Institution(s)

3.5.1. Microindentation Hardness Measurements. Microindentation measurements were performed on the surface as well as the cross section of the coating layers using a 0.098 N and 0.49 N applied loads, respectively. Vickers hardness values are defined as the applied load divided by the actual residual indentation area and obtained according to the equation (2) [ASTM 387-17] as follows:

$$Hv = 1854.4 \times \frac{P}{d^2} \qquad (2)$$

Where P is the load in gf and d is the mean diagonal length of the indentation in μm. Hardness values are also provided in SI unit of GPa.

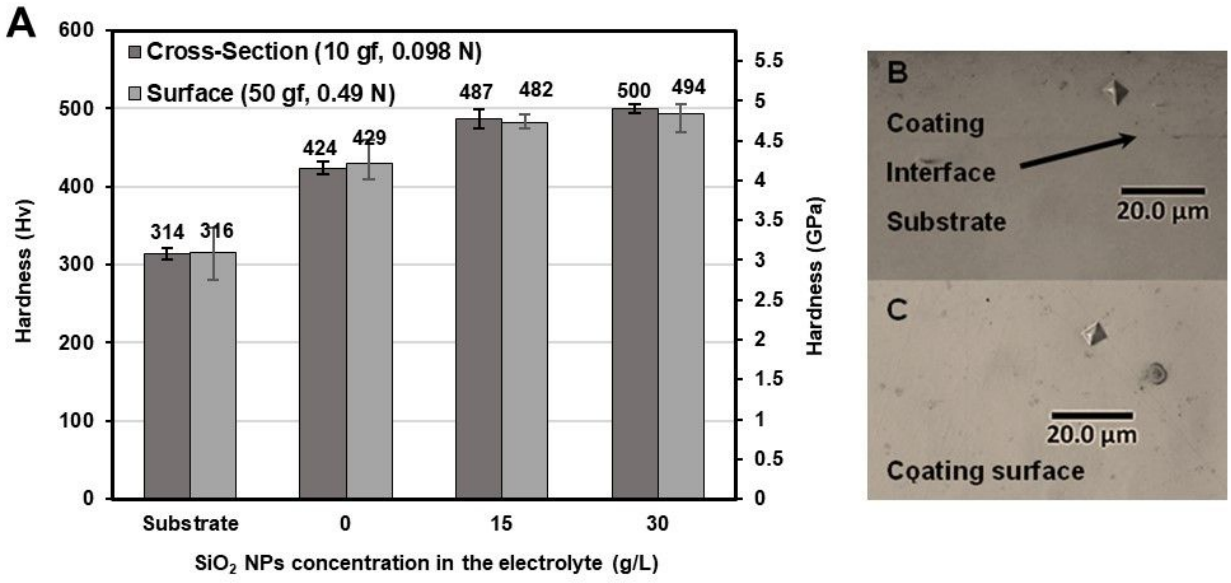

Figure 7. A) Microindentation hardness results performed on the cross-section (dark gray) and surface (light gray), of Ni,[44] and Ni-SiO_2 coatings electrodeposited at 8 mA cm^{-2} from an electrolyte containing 0, 15 and 30 g/L SiO_2 NPs. Microindentation hardness measurements were also performed for the bare polished AISI 1045 substrate, for comparison. B) and C) Optical microscopy micrographs of the microindentation indents performed on the cross section

© The Author(s) or their Institution(s)

and surface of the Ni-SiO_2 coatings electroplated from the electrolyte containing 15 and 30 g/L of SiO_2, respectively. There is no evidence of visible cracks around the indents.

Study of the microindentation hardness values displayed in Figure 7, shows that with the addition of SiO_2 NPs into the electrolyte, cross-section and surface hardness values of the coatings increased further. The maximum hardness is achieved for the coating electroplated from the electrolyte containing 30 g/L of SiO_2 with a value of 4.90 GPa (500 Hv), which is ca. 1.2 and 1.6 times those of the Ni coating (4.16 GPa (424 Hv)) and the bare substrate (3.08 Pa (314 Hv)), respectively.[44] The hardness values obtained from the indentation measurements on the surface and cross-sections of the coatings display the same values and follow the same behavior, although higher applied load was employed to do the indentation measurements on the surface of the coatings compared to the cross-section. This evidence supports the low probability of having load-hardness problem with such coatings, because of the interaction between dislocations and indenter at forces lower than 0.981 N (100 gf) in Vickers hardness measurements [ASTM 387-17].

3.5.2. Nanoindentation Hardness Measurements. Nanoindentation hardness measurements are reported as a bar graph in Figure 8 and compared with the bare substrate. Measurements were performed at least at 10 to 15 different locations on the coating cross-section using a 20 mN maximum load, and the hardness values were calculated based on equation (3),[48]

$$H=L_{max}/A_p \qquad (3)$$

where L_{max} is the maximum peak load and A_p is the residual projected contact area after the unloading step.

Draft

© The Author(s) or their Institution(s)

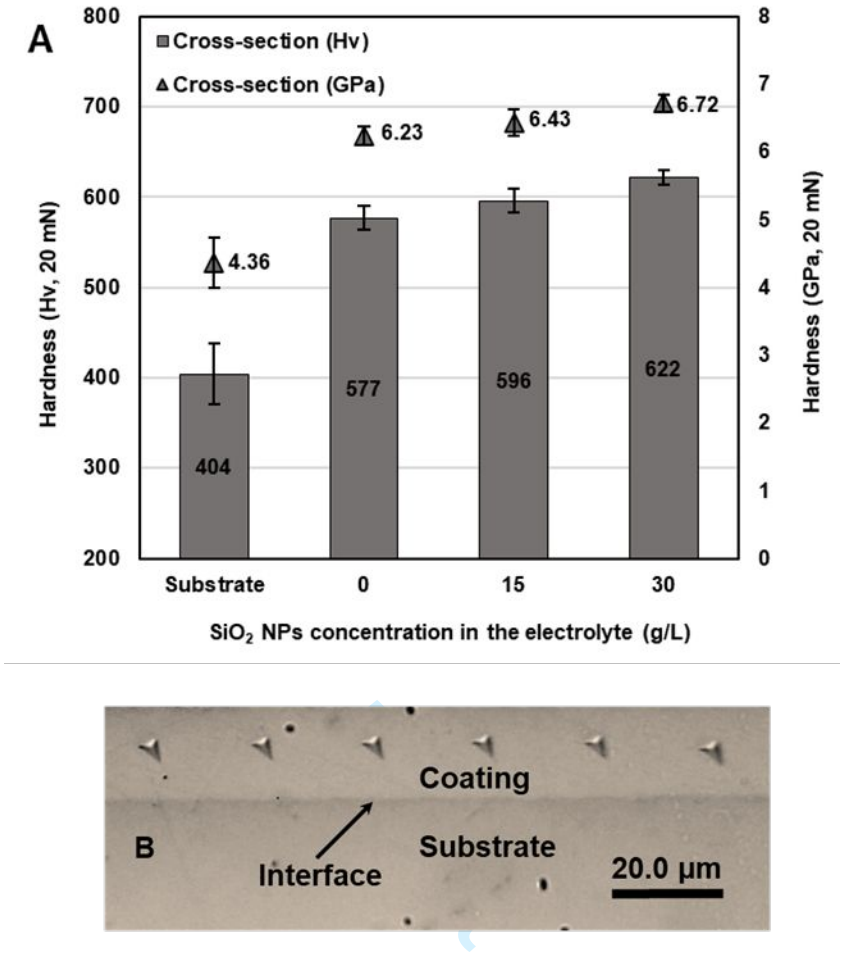

551

552 **Figure 8.** A) Nanoindentation hardness results obtained on the cross-section of coatings
553 electrodeposited from electrolyte containing 0, 15 and 30 g/L SiO_2 NPs by applying 20 mN
554 maximum load. Nanoindentation hardness measurements were also performed for the bare AISI
555 1045 substrate to allow for comparison. B) Optical micrograph of nanoindentation indents
556 performed on the cross-section of Ni coating. The coating-substrate interface is clearly visible,
557 and all indents are confined within the coating region. The average diagonal length of the
558 indents is approximately 2 µm under a maximum applied load of 20 mN, and a large enough
559 spacing between indents ensures that there is no indent proximity effects.

© The Author(s) or their Institution(s)

Figure 8B, shows that all indents are clearly in the coating region, far from the interface between substrate and coating, minimizing the substrate effect on the hardnes values (as explained in section 2.4). The micrographs of the indents show that the edges are smooth without any evidence of radial, lateral or corner cracks. It might be useful to consider higher magnification imaging using SEM and AFM to investigate specifically the cracking, fracture toughness, pile-up or sink-in around the indents in future work.

Comparison of the nanoindentation hardness measurements results in Figure 8 shows that the addition of SiO_2 into the electrolyte caused an increase in hardness. A maximum hardness of 6.72 GPa (622 Hv) obtained for the cross-section of the Ni-SiO_2 coating electroplated from electrolyte containing 30 g/L SiO_2 NPs shows an 8% and 54% increase in hardness compared to the Ni coating (6.23 GPa) and substrate (4.36 GPa), respectively. The nanoindentation hardness measured for Ni coating obtained and reported by Refai *et al.*[63] was 2.8 GPa for a Ni coating electroplated from an alkaline bath and this value increased to 4.8 Gpa with the addition of ZnO into the electrolyte.[63]

Load/indentation depth curves obtained from nanoindentation hardness measurements done on the cross sections of all coatings are explained in section S2.6 and Figure S10 in Supplementary Materials.

*3.5.3. Hardness Enhancement***.** The superior hardness performance of the Ni coating in the absence of SiO_2 NPs compared to the Ni coatings electroplated from Watts type electrolyte reported in other literature,[18,23,64] can be related to the nano sized Ni crystallite in the Ni coating electroplated from DES-based electrolyte[23] and a strengthening mechanism defined by the Hall-Petch relationship.[65] This is explained in details for microindentation hardness measurements in our previous work.[44]

Draft

© The Author(s) or their Institution(s)

583 The higher hardness measured for the Ni-SiO_2 nanocomposite coatings compared to the Ni, can
584 be attributed to the reinforcement effect of the NPs on the Ni matrix strength. The incorporation
585 of SiO_2 NPs in the Ni matrix can act as obstacles impeding the movement of the dislocations.
586 Dislocations resistance against bowing, between obstacles (such as NPs), result in hardness
587 improvement through a dispersion strengthening mechanism based on the Orowan
588 mechanism[35,66] (see additional explanation in section S2.6). This characteristic of
589 nanocomposite coatings can result in a hardness improvement because of the impact of
590 additional resistance to the plastic deformation of the Ni matrix resulting from the accumulation
591 of dislocation at the boundaries. Under an applied load, dislocation loops will be created, then
592 they will pile up at the grain boundaries adding resistance against the plastic deformation until
593 dislocation in the adjacent grains is initiated and plastic deformation takes place.[65,67] The plastic
594 deformation $_{and}$ strengthening behavior versus grain size is defined by the Hall-Petch
595 relationship.[65,67] According to this relationship the hardness of the material is related to the
596 reciprocal of the square root of the grain size based on the equation (4),[68]

597 $$H_{g.s} = H_0 + K\, d^{(-1/2)} \qquad (4)$$

598 where $H_{g.s}$ is the hardness contribution of grain size, H_0, K and d, are the intrinsic hardness,
599 material constant and the measured grain size of the material, respectively.
600 Measured micro- and nano-indentation hardness values obtained from the cross-section of the
601 coatings are plotted versus $d^{(-1/2)}$ and displayed in Figure 9 in the form of Hall-Petch
602 relationship. It can be assumed that the overall coating hardness measured here, consists of
603 different hardness contribution from: incorporated nano particles in the Ni matrix ($H_{inc.}$), grain
604 size refinement ($H_{g.s.}$) and cluster size refinement ($H_{c.s.}$), according to the equation (5):

605 $$\text{Measured hardness (H)} = H_{inc.} + H_{g.s.} + H_{c.s.} \qquad (5)$$

© The Author(s) or their Institution(s)

606 It has been shown that the addition of NPs to the matrix and grain size refinement favor the
607 formation of pores in the coatings.[58,69] Hence based on the results obtained by Ma *et al.*,[70] it can
608 be said that $H_{inc.}$, $H_{g.s.}$, and $H_{c.s.}$ in equation (5) are the balanced hardness contribution of a)
609 silica incorporation and pores, b) grain size refinement and pores, and c) cluster size refinement
610 and pores, respectively.
611

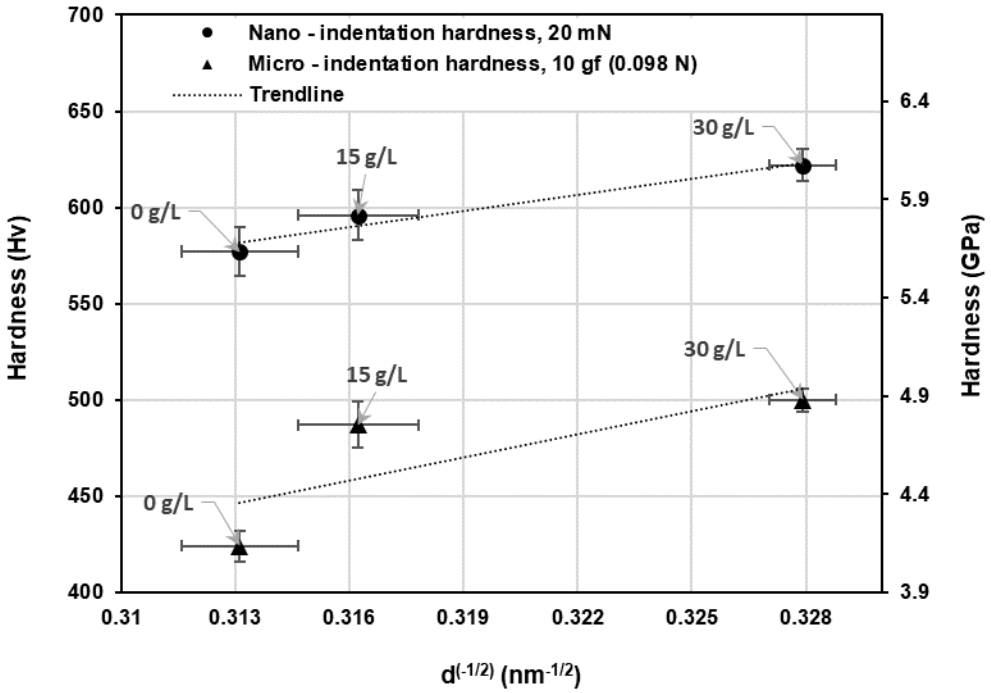

612

613 **Figure 9.** Measured cross-sectional micro- and nanoindentation hardness values versus the
614 inverse of the square roots of the average grain size (obtained by using Debye-Scherrer
615 equation). Hall–Petch trend plot showing the relationship between hardness and grain size in
616 Ni-SiO_2 nanocomposites. While only three data points are available, the results exhibit the
617 expected increase in hardness with decreasing grain size (trendlines represent the linear
618 regression), consistent with Hall–Petch behavior.

© The Author(s) or their Institution(s)

Figure 9 illustrates the variation of micro- and nano- indentation hardness as a function of the inverse square root of grain size for Ni and Ni–SiO_2 nanocomposites. When comparing the coating prepared witout and with 30g/L SiO_2 NPs, the hardness increases with decreasing grain size, where the average grain sizes are 9.3 ± 0.1 nm and 10 ± 0.2 nm for the for Ni and Ni-SiO_2 coating (prepared with 30 g/L SiO_2), respectively. This trend is consistent with the classical Hall–Petch relationship, which describes grain boundary strengthening due to the impediment of dislocation motion by grain boundaries. Importantly, there is no indication of the inverse Hall–Petch effect, which typically emerges at grain sizes below 10 nm.[65,71] This suggests that the grain size (down to 9.3 ±0.1 nm) remain within the range where grain boundary strengthening dominates. This contrasts with previous findings for pure Ni coatings electrodeposited under the same conditions but without SiO_2 NPs, where the inverse Hall–Petch behavior was observed and explained.[44]

The enhancement in both micro- and nanoindentation hardness upon the addition of 15 g/L SiO_2 NPs to the electrolyte can be attributed to a combination of factors: NP incorporation, grain size refinement, and cluster size reduction. In our study the average grain size remains the same 10.2 ± 0.2 nm and 10.0 ± 0.2 nm (Section 3.2) for these two conditions. Therefore, the observed hardness improvement is more likely governed by dispersion and dislocation strengthening from the embedded NPs and by the reduction in cluster size, which can hinder dislocation motion more effectively.

Nanoindentation hardness is a measurement that reflect the hardness in grains and grain boundaries whereas microindentation measures hardness over a larger area, integrating responses from a broader microstructural region.[72] Consequently, the refinement of microscale clusters is expected to have a more pronounced effect on microindentation hardness than in the

Draft

© The Author(s) or their Institution(s)

case of nanoindentation. This explains the more significant increase in microindentation hardness relative to nanoindentation hardness versus $d^{-1/2}$ in Figure 9 following the addition of 15 g/L SiO_2. This behavior highlights the role of cluster size refinement in enhancing hardness at larger length scales.

With an increase in the concentration of SiO_2 from 15 to 30 g/L in the electrolyte, the micro- and nanoindentation hardness continue to increase versus $d^{-1/2}$, though at a reduced rate. This suggests a diminished contribution of the embedded NPs to hardness enhancement at higher concentration of 30 g/L of SiO_2. Previous studies have shown that increasing NP content in the electrolyte raises the likelihood of pore formation in the coating, which adversely affects mechanical properties.[69] This may account for the reduced effectiveness of NP incorporation on hardness at 30 g/L. Additionally, the similar trends observed in micro- and nanoindentation hardness suggest a limited influence of cluster size refinement at this concentration. This interpretation is supported by SEM (Sections 3.4 ; Figures 3d, e, g, h), which show no significant changes in cluster size between the coatings deposited from electrolytes containing 15 and 30 g/L SiO_2. Therefore, the hardness increase versus $d^{-1/2}$ at 30 g/L SiO_2 appears primarily governed by the reduction in Ni crystallite size (from 10.2 ± 0.2 nm to 9.3 ± 0.1 nm, Section 3.2) and continued NP incorporation.

3.6. Potentiodynamic polarization

Potentiodynamic polarization results for Ni coating and Ni-SiO_2 electrodeposited with silica concentration of 15 and 30 g/L are presented in Figure 10 and summarized in Table 2. A drawing of the electrochemical cell used for potentiodynamic polarization is shown in Figure S11, Section S2.7. The influence of aging in air on the Ni coating corrosion properties has been discussed in a previous study.[44] Therefore, the polarization experiments in the present work were

Draft

© The Author(s) or their Institution(s)

performed on freshly electroplated surfaces. To assess the impact of surface defects and roughness on corrosion behavior, additional polarization experiments were carried out after a gentle polishing of the coatings. The polishing procedure, described in section S.1.3. of the Supplementary Materials, employed Struers MD-Nap cloth and a DiaPro Nap B 1 μm suspension to avoid any aluminum or silicon contaminants on the polished surfaces. The micrograph of the cross section after polishing is shown in Figure 10 C, representing undamaged layer.

A comparison of the results indicates that the addition of silica NPs up to 15 g/L led to a positive shift in the corrosion potential. However, the corrosion current density increased for coatings electrodeposited from electrolytes containing 15 and 30 g/L of silica NPs, compared to the pure Ni coating. After polishing, to reduce surface roughness and eliminate surface defects, the corrosion potential of all coatings shifted in the positive direction, while the corrosion current density decreased significantly—by factors of approximately 3.5, 70, and 60 for coatings containing 0, 15, and 30 g/L of silica NPs, respectively. This improvement is attributed to the reduced exposed surface area and the diminished presence of surface defects after polishing. The formation of the passive layer was notably enhanced following surface polishing, particularly in the coating deposited from the electrolyte containing 15 g/L of SiO_2 NPs. This enhancement is likely due to the smoother surface promoting the development of a more uniform and continuous passive film. Moreover, the presence of ceramic NPs facilitated the formation of a more stable, uniform and protective passive layer by promoting passivation behavior in the nanocomposite coating.[73]

Evaluation and comparison of the polarization behavior of Ni and Ni–SiO_2 composite coatings before and after polishing provide a better understanding of the influence of embedded NPs on

© The Author(s) or their Institution(s)

corrosion behavior, isolating the effect of surface roughness and texture. Among the coatings studied, the one electrodeposited from the electrolyte containing 15 g/L of silica NPs exhibited the most positive corrosion potential and the lowest corrosion current density. This markedly improved polarization behavior can be attributed to the enhanced barrier properties, reduced porosity, and improved pitting resistance imparted by the silica NPs. Acting as a more noble phase compared to the Ni matrix, the silica NPs contributed to the positive shift in corrosion potential observed in the nanocomposite coatings.

Additionally, the incorporation of NPs resulted in a reduction in grain cluster size and overall grain size (see section 3.2, and Figure 3), leading to an increased number of grain boundaries that act as barriers to corrosion propagation.[73] The possibly incorporation of NPs at grain boundaries intersections and defect sites may also mitigate the detrimental effects of surface imperfections on corrosion resistance.[74]

However, comparison of the potentiodynamic polarization behavior of Ni-SiO_2 coatings electroplated from the electrolyte containing 15 and 30 g/L SiO_2 NPs, revealed a less positive corrosion potential and a higher corrosion current density when the NP concentration in the electrolyte was increased from 15 to 30 g/L. This trend is likely due to the increased probability of defect and pore formation at higher NP concentrations. These observations are consistent with the micro- and nanoindentation hardness results discussed for Ni-SiO_2 electrodeposited from the electrolyte containing 30 g/L SiO_2 NPs, in Section 3.5.3.

Draft

© The Author(s) or their Institution(s)

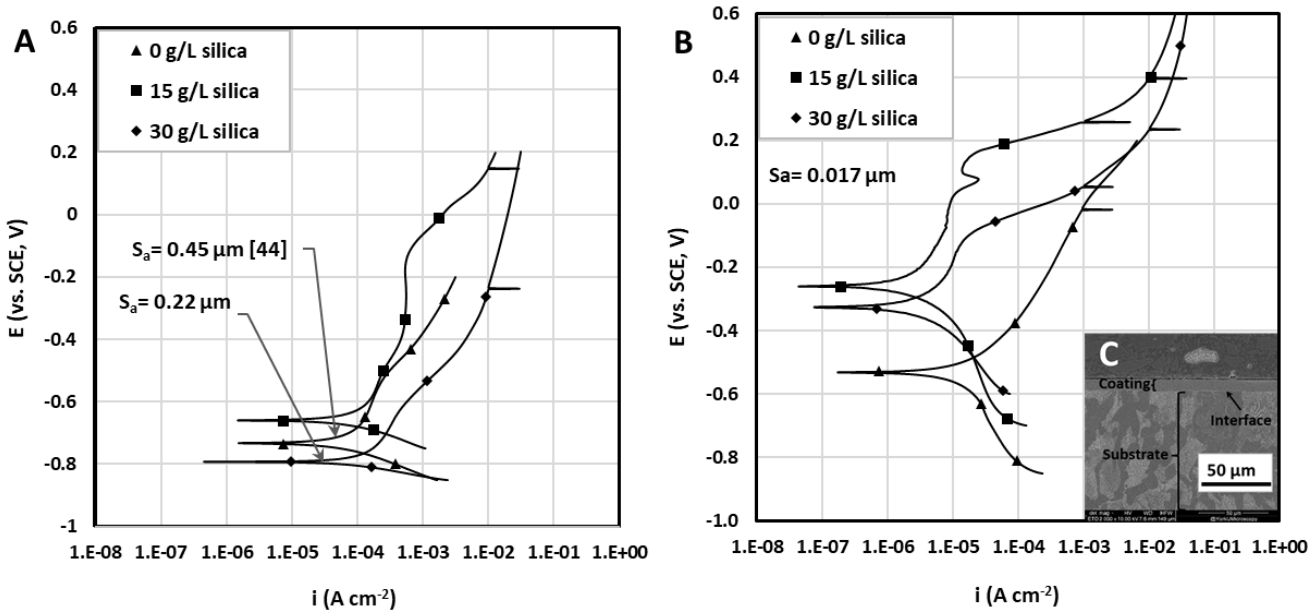

Figure 10. Potentiodynamic polarization behavior of coating layers deposited with different concentration of SiO_2 NPs in the electrolyte (0, 15, and 30 g/L): A) before polishing and B) after polishing (Sa reduced to about 0.017 µm for all three coatings). S_a denotes the surface roughness, representing the arithmetical mean height of the selected area (see Figure S9 and Table S1, Supplementary Materials). Note that the symbols are used solely to identify the samples. The continuous lines were obtained from closely spaced data points. C) SEM micrograph of the Ni coating surface after gentle polishing to reduce surface roughness and defects. The coating thickness slightly decreased due to poilishing; however, the layer remains continuous and undamaged.

Draft

© The Author(s) or their Institution(s)

Table 2. Potentiodynamic polarization results of Ni and Ni-SiO_2 coatings electrodeposited from the electrolyte containing 0, 15, and 30 g/L of SiO_2 NPs and the bare substrate.

Surface finishing	SiO_2 concentration in the electrolyte (g/L)	S_a (μm)	E_{Corr} vs. SCE (mV)	i_{Corr} (μA cm^{-2})	R_p (Ω cm^2)
Unpolished	0	0.45[44]	-736[44]	79[44]	118[44]
Unpolished	15	-	-663	126 ± 9	228 ± 10
Unpolished	30	0.22	-792	176 ± 18	171 ± 17
Polished	0	~ 0.017	-532	17 ± 3	2445 ± 177
Polished	15	~ 0.017	-260	2.6 ± 0.6	15211 ± 388
Polished	30	~ 0.017	-327	3.6 ± 0.6	10570 ± 116
—	Bare substrate	~ 0.017[44]	-648[44]	43[44]	599[44]

4. Conclusions

Electrodeposition of Ni and Ni-SiO_2 nanocomposite coatings from ethaline-based electrolyte led to the fabrication of nanostructured Ni and nanocomposite coatings. The addition of NPs did not affect the overall texture or Ni crystallographic planes, where all coatings display a fcc unit cell with peaks detected for the (111), (200), (220) and (311) crystallographic planes. The grain size measurements revealed a decrease of Ni grain size with the increase of NPs concentration from 0 to 30 g/L in the electrolyte. All coating surfaces displayed granular growth with platelets formation out of the surface plane and grains forming cauliflower-liked clusters. The presence of the SiO_2 NPs in the electrolyte promoted the development of a more regular coating morphology and surface texture with less irregularity and more normal heigh distribution compared to that of nickel. A higher hardness (18% for microindentation hardness and 8% for nanoindentation hardness) was obtained for the coating electroplated from electrolyte containing 30 g/L of silica, with respect to that of Ni through dispersion and dislocation strengthening mechanisms, respectively. The addition of SiO_2 NPs to the Ni coating yieled a

Draft

© The Author(s) or their Institution(s)

hardness versus the reciprocal of the square root of the grain size that follows the Hall-Petch trend and no evidence of softening effect was observed. The addition of 15 g/L SiO_2 NPs in the electrolye caused a positive shift in the corrosion potential compared to the Ni SiO_2-free coating. Further improve of polarization behavior was observed after polishing for all coatings in the presence and absence of NPs. Corrosion current density reduced by factor of 11 and 7 with the addition of 15 and 30 g/L SiO_2 NPs, respectively. Environmentally friendly deep eutectic solution, ethaline-based electrolyte, was successfully used to develop high performance Ni and reinforced Ni-SiO_2 composite coatings with improved corrosion and surface hardness properties.

Declaration of competing interests

The authors declare that they have no known competing financial interests or personal relationships that could have appeared to influence the work reported in this paper.

CRediT author contribution statement

Mehry Fattah: Conceptualization, Methodology, Software, Formal analysis, Investigation, Resources, data curation, Visualization, Writing- Original draft preparation, Writing- Reviewing and Editing. Sylvie Morin: Methodology, Supervision, Funding acquisition, Writing- Reviewing and Editing.

Acknowledgment

York University is acknowledged for the support of this research. Dr. Magdalena Jaklewicz at York University, Imaging Facility, for SEM and EDX measurements and analysis. Victoria

© The Author(s) or their Institution(s)

Jarvis, Dr. Jim Britten and Maureen Fitzpatrick at McMaster University, Analytical X-ray Diffraction Facility, for XRD measurements and X-ray pattern analysis. Dr. Zeynel Bayindir, Biointerfaces Institute, McMaster University, for XPS measurements, and Dr. Mark Biesinger, Surface Science Western, for his advice with XPS data analysis. Shariful Islam from the Material Property Assessment Laboratory (MPAL) at McMaster University for hardness and topography measurements.

Data availability

The raw/processed data required to reproduce these findings can be shared upon request.

Funding Sources

York University, Toronto, ON, Canada.

Draft

Supplementary Materials

Supplementary Materials to this article can be found online at:

References

(1) Liu, C.; Bi, Q.; Layland, A.; Matthews, A. An electrochemical impedance spectroscopy study of the corrosion behaviour PVD coated steels in 0.5 N NaCl aqueous solution: Part II. EIS interpretation of corrosion behaviour. *Corros. Sci.* **2003**, *45* (6), 1257–1273. https://doi.org/10.1016/S0010-938X(02)00214-7

(2) Hoche, H.; Pusch, C.; Oechsner, M. Corrosion and wear protection of mild steel substrates by innovative PVD coatings. *Surf. Coat. Technol*. **2020**, *391*, 125659. https://doi.org/10.1016/j.surfcoat.2020.125659

(3) Siddiqui, A.R.; Maurya, R.; Katiyar, P.K.; Balani, K. Superhydrophobic, self-cleaning carbon nanofiber CVD coating for corrosion protection of AISI 1020 steel and AZ31 magnesium alloys. *Surf. Coat. Technol*. **2020**, *404*, 126421. https://doi.org/10.1016/j.surfcoat.2020.126421

© The Author(s) or their Institution(s)

(4) Abidin, A. Z.; Kozera, R.; Höhn, M.; Endler, I.; Knaut, M.; Boczkowska, A.; Czulak, A.; Malczyk, P.; Sobczak, N.; Michaelis, A. Preparation and characterization of CVD-TiN-coated carbon fibers for applications in metal matrix composites. *Thin Solid Films* **2015**, *589*, 479–486. https://doi.org/10.1016/j.tsf.2015.06.022

(5) Baranov, O.; Fang, J.; Ostrikov, K. (Ken); Cvelbar, U. TiN deposition and morphology control by scalable plasma-assisted surface treatments. *Mater. Chem. Phys*. **2017**, *188*, 143–153. https://doi.org/10.1016/j.matchemphys.2016.12.010

(6) Spanou, S.; Kontos, A.I.; Siokou, A.; Kontos, A.G.; Vaenas, N.; Falaras, P.; Pavlatou, E.A. Self cleaning behaviour of Ni/nano-TiO_2 metal matrix composites. *Electrochim. Acta* **2013**, *105*, 324–332. https://doi.org/10.1016/j.electacta.2013.04.174.

(7) Benea, L.; Bonora, P.L.; Borello, A.; Martelli, S.; Wenger, F.; Ponthiaux, P.; Galland, J. Preparation and investigation of nanostructured SiC-nickel layers by electrodeposition. *Solid State Ionics* **2002**, *151*, 89–95. www.elsevier.com/locate/ssi

(8) Li, X.; Yin, S.; Luo, H. Fabrication of robust superhydrophobic Ni–SiO_2 composite coatings on aluminum alloy surfaces. *Vacuum* **2020**, *181*, 109674. https://doi.org/10.1016/j.vacuum.2020.109674.

(9) Khorsand, S.; Raeissi, K.; Ashrafizadeh, F. Corrosion resistance and long-term durability of superhydrophobic nickel film prepared by electrodeposition process. *Appl. Surf. Sci.* **2014,** *305,* 498–505. https://doi.org/10.1016/j.apsusc.2014.03.123

(10) Hang, T.; Hu, A.; Ling, H.; Li, M.; Mao, D. Superhydrophobic nickel films with micro-nano hierarchical structure prepared by electrodeposition. *Appl. Surf. Sci.* **2010,** *256,* 2400–2404. https://doi.org/10.1016/j.apsusc.2009.10.074

(11) Baik, D. S.; Fray, D. J. Electrodeposition of zinc from high acid zinc chloride solutions. *J. Appl. Electrochem.* **2001,** *31,* 1141–1147. https://doi.org/10.1023/A:1012290132379

(12) Gomes, A.; Da Silva Pereira, M. I. Pulsed electrodeposition of Zn in the presence of surfactants. *Electrochim. Acta* **2006,** *51,* 1342–1350. https://doi.org/10.1016/j.electacta.2005.06.023

(13) Huang, S.; Hu, Y.; Pan, W. Relationship between the structure and hydrophobic performance of Ni–TiO_2 nanocomposite coatings by electrodeposition. *Surf. Coat. Technol.* **2011,** *205,* 3872–3876. https://doi.org/10.1016/j.surfcoat.2011.01.065

(14) Mohajeri, S.; Dolati, A.; Ghorbani, M. An investigation on the electrodeposition mechanism of Ni–TiO_2 nanocomposite coatings. *J. Ultrafine Grained Nanostruct. Mater.* **2016,** *49,* 51–63. https://doi.org/10.7508/jufgnsm.2016.02.01

(15) Kasturibai, S.; Kalaignan, G. P. Physical and electrochemical characterizations of Ni–SiO_2 nanocomposite coatings. *Ionics* **2013,** *19,* 763–770. https://doi.org/10.1007/s11581-012-0810-0

Draft

© The Author(s) or their Institution(s)

(16) Liu, Y.; Yu, S. R.; Liu, J. D.; Han, Z. W.; Yuan, D. S. Microstructure and wear resistance of electrodeposited Ni–SiO_2 nanocomposite coatings on AZ91HP magnesium alloy substrate. *Trans. Nonferrous Met. Soc. China* **2011,** *21,* S483–S488. https://doi.org/10.1016/S1003-6326(11)61629-4

(17) Ali, K.; Narayana, S.; Shakoor, R. A.; Okonkwo, P. C.; Yusuf, M. M.; Alashraf, A.; Kahraman, R. Synthesis and performance evaluation of pulse electrodeposited Ni–AlN nanocomposite coatings. *Scanning* **2018,** *2018* (1), 7187024. https://doi.org/10.1155/2018/7187024

(18) Tsongas, K.; Tzetzis, D.; Karantzalis, A.; Banias, G.; Exarchos, D.; Ahmadkhaniha, D.; Zanella, C.; Matikas, T.; Bochtis, D. Microstructural, surface topology and nanomechanical characterization of electrodeposited Ni–P/SiC nanocomposite coatings. *Appl. Sci.* **2019,** *9,* 2901. https://doi.org/10.3390/app9142901

(19) Borkar, T.; Harimkar, S. P. Effect of electrodeposition conditions and reinforcement content on microstructure and tribological properties of nickel composite coatings. *Surf. Coat. Technol.* **2011,** *205,* 4124–4134. https://doi.org/10.1016/j.surfcoat.2011.02.057

(20) Azem, F. A. K.; Birlik, I.; Koc Delice, T.; Dalmis, R. Corrosion performance of electrodeposited Ni nanocomposite coatings reinforced with metal oxide particles. *DEU Fac. Eng. J. Sci. Eng.* **2024,** *26,* 28–33. https://doi.org/10.21205/deufmd.2024267604

(21) Abbott, A. P.; Boothby, D.; Capper, G.; Davies, D. L.; Rasheed, R. K. Deep eutectic solvents formed between choline chloride and carboxylic acids: Versatile alternatives to ionic liquids. *J. Am. Chem. Soc.* **2004,** *126,* 9142–9147. https://doi.org/10.1021/ja048266j

(22) Gu, C.; Tu, J. One-step fabrication of nanostructured Ni film with lotus effect from deep eutectic solvent. *Langmuir* **2011,** *27,* 10132–10140. https://doi.org/10.1021/la200778a

(23) Abbott, A. P.; Ballantyne, A.; Harris, R. C.; Juma, J. A.; Ryder, K. S. A comparative study of nickel electrodeposition using deep eutectic solvents and aqueous solutions. *Electrochim. Acta* **2015,** *176,* 718–726. https://doi.org/10.1016/j.electacta.2015.07.051

(24) Abbott, A. P.; Ballantyne, A.; Harris, R. C.; Juma, J. A.; Ryder, K. S. Bright metal coatings from sustainable electrolytes: The effect of molecular additives on electrodeposition of nickel from a deep eutectic solvent. *Phys. Chem. Chem. Phys.* **2017,** *19,* 3219–3231. https://doi.org/10.1039/c6cp08720e

(25) Protsenko, V. S.; Kityk, A. A.; Shaiderov, D. A.; Danilov, F. I. Effect of water content on physicochemical properties and electrochemical behavior of ionic liquids containing choline chloride, ethylene glycol and hydrated nickel chloride. *J. Mol. Liq.* **2015,** *212,* 716–722. https://doi.org/10.1016/j.molliq.2015.10.028

(26) Lukaczynska, M.; Mernissi Cherigui, E. A.; Ceglia, A.; Van Den Bergh, K.; De Strycker, J.; Terryn, H.; Ustarroz, J. Influence of water content and applied potential on the

© The Author(s) or their Institution(s)

electrodeposition of Ni coatings from deep eutectic solvents. *Electrochim. Acta* **2019,** *319,* 690–704. https://doi.org/10.1016/j.electacta.2019.06.161

(27) Mernissi Cherigui, E. A.; Sentosun, K.; Bouckenooge, P.; Vanrompay, H.; Bals, S.; Terryn, H.; Ustarroz, J. Comprehensive study of the electrodeposition of nickel nanostructures from deep eutectic solvents: Self-limiting growth by electrolysis of residual water. *J. Phys. Chem. C* **2017,** *121,* 9337–9347. https://doi.org/10.1021/acs.jpcc.7b01104

(28) Cui, J.; Sun, H.; Tan, Y.; Zhou, X.; Wang, B.; Sun, J. Electrodeposition of Ni from choline chloride/ethylene glycol deep eutectic solvent and pure ethylene glycol. *JOM* **2024,** *76,* 2178–2188. https://doi.org/10.1007/s11837-024-06456-y

(29) Barrera, P. R.; Rodríguez, C. E.; Gomez, F. J. R. Comparative assessment of Ni–Co coatings obtained from a deep eutectic solvent, choline chloride–ethylene glycol, and water by electroplating. *J. Solid State Electrochem.* **2023,** *27,* 3075–3089. https://doi.org/10.1007/s10008-023-05591-x

(30) Li, R.; Hou, Y.; Liu, B.; Wang, D.; Liang, J. Electrodeposition of homogenous Ni/SiO_2 nanocomposite coatings from deep eutectic solvent with in situ synthesized SiO_2 nanoparticles. *Electrochim. Acta* **2016,** *222,* 1272–1280. https://doi.org/10.1016/j.electacta.2016.11.101

(31) Li, R.; Hou, Y.; Liang, J. Electro-codeposition of Ni–SiO_2 nanocomposite coatings from deep eutectic solvent with improved corrosion resistance. *Appl. Surf. Sci.* **2016,** *367,* 449–458. https://doi.org/10.1016/j.apsusc.2016.01.241

(32) Li, R.; Chu, Q.; Liang, J. Electrodeposition and characterization of Ni–SiC composite coatings from deep eutectic solvent. *RSC Adv.* **2015,** *5,* 44933–44942. https://doi.org/10.1039/c5ra05918f

(33) Wesley, W. A.; Roehl, E. J. The electrodeposition of hard nickel. *Trans. Electrochem. Soc.* **1942,** *82,* 1–16. https://doi.org/10.1149/1.3071397

(34) Danilov, F. I.; Kityk, A. A.; Shaiderov, D. A.; Bogdanov, D. A.; Korniy, S. A.; Protsenko, V. S. Electrodeposition of Ni–TiO_2 composite coatings using electrolyte based on a deep eutectic solvent. *Surf. Eng. Appl. Electrochem.* **2019,** *55,* 138–149. https://doi.org/10.3103/S106837551902008X

(35) Hou, F.; Wang, W.; Guo, H. Effect of the dispersibility of ZrO_2 nanoparticles in Ni–ZrO_2 electroplated nanocomposite coatings on the mechanical properties of nanocomposite coatings. *Appl. Surf. Sci.* **2006,** *252,* 3812–3817. https://doi.org/10.1016/j.apsusc.2005.05.076

(36) Rosoiu, S. P.; Pantazi, A. G.; Petica, A.; Cojocaru, A.; Costovici, S.; Zanella, C.; Visan, T.; Anicai, L.; Enachescu, M. Comparative study of Ni–Sn alloys electrodeposited from

© The Author(s) or their Institution(s)

choline chloride-based ionic liquids in direct and pulsed current. *Coatings* **2019,** *9,* 801. https://doi.org/10.3390/coatings9120801

(37) Ashassi-Sorkhabi, H.; Hagrah, A.; Parvini-Ahmadi, N.; Manzoori, J. Zinc–nickel alloy coatings electrodeposited from a chloride bath using direct and pulse current. *Surf. Coat. Technol.* **2001,** *140,* 278–283. https://doi.org/10.1016/S0257-8972(01)01032-5

(38) Pingale, A. D.; Owhal, A.; Belgamwar, S. U.; Rathore, J. S. Effect of current on the characteristics of CuNi-G nanocomposite coatings developed by DC, PC, and PRC electrodeposition. *JOM* **2021,** *73,* 4299–4308. https://doi.org/10.1007/s11837-021-04815-7

(39) Arunsunai Kumar, K.; Paruthimal Kalaignan, G.; Muralidharan, V. S. Direct and pulse current electrodeposition of Ni–W–TiO_2 nanocomposite coatings. *Ceram. Int.* **2013,** *39,* 2827–2834. https://doi.org/10.1016/j.ceramint.2012.09.054

(40) Imanian Ghazanlou, S.; Farhood, A. H. S.; Ahmadiyeh, S.; Ziyaei, E.; Rasooli, A.; Hosseinpour, S. Characterization of pulse and direct current methods for electrodeposition of Ni–Co composite coatings reinforced with nano- and micro-ZnO particles. *Metall. Mater. Trans. A* **2019,** *50,* 1922–1935. https://doi.org/10.1007/s11661-019-05118-y

(41) Yang, Y.; Cheng, Y. F. Fabrication of Ni–Co–SiC composite coatings by pulse electrodeposition – Effects of duty cycle and pulse frequency. *Surf. Coat. Technol.* **2013,** *216,* 282–288. https://doi.org/10.1016/j.surfcoat.2012.11.059

(42) Jiang, S.; Guo, Z.; Deng, Y.; Dong, H.; Li, X.; Liu, J. Effect of pulse frequency on the one-step preparation of superhydrophobic surface by pulse electrodeposition. *Appl. Surf. Sci.* **2018,** *458,* 603–611. https://doi.org/10.1016/j.apsusc.2018.07.120

(43) Li, H.; He, Y.; Luo, P.; Fan, Y.; Yu, H.; Wang, Y.; He, T.; Li, Z.; Zhang, H. Influence of pulse frequency on corrosion resistance and mechanical properties of Ni–W/B_4C composite coatings. *Colloids Surf., A* **2021,** *629,* 127436. https://doi.org/10.1016/j.colsurfa.2021.127436

(44) Fattah, M.; Morin, S. Microstructure, corrosion and hardness properties of Ni coatings electrodeposited from a deep eutectic solvent-based electrolyte. *J. Mater. Eng. Perform.* **2024.** https://doi.org/10.1007/s11665-024-10565-9

(45) Abbott, A. P.; El Ttaib, K.; Ryder, K. S.; Smith, E. L. Electrodeposition of nickel using eutectic based ionic liquids. *Trans. Inst. Met. Finish.* **2008,** *86,* 234–240. https://doi.org/10.1179/174591908X327581

(46) Abbott, A. P.; Barron, J. C.; Frisch, G.; Gurman, S.; Ryder, K. S.; Silva, A. F. Double layer effects on metal nucleation in deep eutectic solvents. *Phys. Chem. Chem. Phys.* **2011,** *13,* 10224–10231. https://doi.org/10.1039/c0cp02244f

Draft

© The Author(s) or their Institution(s)

(47) Fairley, N.; Fernandez, V.; Richard-Plouet, M.; Guillot-Deudon, C.; Walton, J.; Smith, E.; Flahaut, D.; Greiner, M.; Biesinger, M.; Tougaard, S.; Morgan, D.; Baltrusaitis, J. Systematic and collaborative approach to problem solving using X-ray photoelectron spectroscopy. *Appl. Surf. Sci. Adv.* **2021,** *5,* 100112. https://doi.org/10.1016/j.apsadv.2021.100112

(48) Zotov, N.; Bartsch, M.; Eggeler, G. Thermal barrier coating systems – Analysis of nanoindentation curves. *Surf. Coat. Technol.* **2009,** *203,* 2064–2072. https://doi.org/10.1016/j.surfcoat.2009.02.008

(49) Oliver, W. C.; Pharr, G. M. An improved technique for determining hardness and elastic modulus using load and displacement sensing indentation experiments. *J. Mater. Res.* **1992,** *7,* 1564–1583.

(50) Rudnik, E.; Burzyńska, L.; Dolasiński, Ł.; Misiak, M. Electrodeposition of nickel/SiC composites in the presence of cetyltrimethylammonium bromide. *Appl. Surf. Sci.* **2010,** *256,* 7414–7420. https://doi.org/10.1016/j.apsusc.2010.05.082

(51) Webb, P. R.; Robertson, N. L. Electrolytic codeposition of Ni/Al_2O_3 thin films. *J. Electrochem. Soc.* **1994,** *141,* 2054789. https://doi.org/10.1149/1.2054789

(52) Roventi, G.; Bellezze, T.; Fratesi, R. Electrodeposition of Zn–SiC nanocomposite coatings. *J. Appl. Electrochem.* **2013,** *43,* 839–846. https://doi.org/10.1007/s10800-013-0571-0

(53) Wasekar, N. P.; Latha, S. M.; Ramakrishna, M.; Rao, D. S.; Sundararajan, G. Pulsed electrodeposition and mechanical properties of Ni–W/SiC nano-composite coatings. *Mater. Des.* **2016,** *112,* 140–150. https://doi.org/10.1016/j.matdes.2016.09.070

(54) Gao, J.; Jie, W.; Yuan, Y.; Wang, T.; Zha, G.; Tong, J. Dependence of film texture on substrate and growth conditions for CdTe films deposited by close-spaced sublimation. *J. Vac. Sci. Technol., A* **2011,** *29,* 3610177. https://doi.org/10.1116/1.3610177

(55) Langford, J. I.; Wilson, A. J. C. Scherrer after Sixty Years: A survey and some new results in the determination of crystallite size. *J. Appl. Crystallogr.* **1978,** *11,* 102–113. https://doi.org/10.1107/S0021889878012844

(56) Gül, H.; Uysal, M.; Akbulut, H.; Alp, A. Effect of PC electrodeposition on the structure and tribological behavior of Ni–Al_2O_3 nanocomposite coatings. *Surf. Coat. Technol.* **2014,** *258,* 1202–1211. https://doi.org/10.1016/j.surfcoat.2014.07.002

(57) Wang, Y.; Zheng, X.; Li, X. Effect of polyethylene glycol molecular weight on the electrodeposition of nanostructured nickel. *Appl. Surf. Sci.* **2023,** *623,* 156886. https://doi.org/10.1016/j.apsusc.2023.156886

(58) Bhardwaj, M.; Balani, K.; Balasubramaniam, R.; Pandey, S.; Agarwal, A. Effect of current density and grain refining agents on pulsed electrodeposition of nanocrystalline

Draft

© The Author(s) or their Institution(s)

nickel. *Surf. Eng.* **2011,** *27,* 642–648. https://doi.org/10.1179/026708410X12683118611185

(59) Jegan, A.; Venkatesan, R.; Arunachalam, R. Mechanical properties of Ni–nano-Al_2O_3 composite coatings on AISI 304 stainless steel by pulsed electrodeposition. *Sci. Eng. Compos. Mater.* **2014,** *21,* 351–358. https://doi.org/10.1515/secm-2013-0071

(60) Fazlolahzadeh, O.; Rouhollahi, A.; Dolati, A.; Ghahramanifard, F. Communication—Co-electrodeposition of Ni/$SiO_2(CH_2)_3SH$ composite: Modified Guglielmi's model and mechanism of nucleation. *J. Electrochem. Soc.* **2017,** *164,* E472–E474. https://doi.org/10.1149/2.1081713jes

(61) Abbott, A. P.; Azam, M.; Ryder, K. S.; Saleem, S. In situ electrochemical digital holographic microscopy: A study of metal electrodeposition in deep eutectic solvents. *Anal. Chem.* **2013,** *85,* 6653–6660. https://doi.org/10.1021/ac400262c

(62) Ustarroz, J.; Hammons, J. A.; Altantzis, T.; Hubin, A.; Bals, S.; Terryn, H. A generalized electrochemical aggregative growth mechanism. *J. Am. Chem. Soc.* **2013,** *135,* 11550–11561. https://doi.org/10.1021/ja402598k

(63) Refai, M.; Hamid, Z. A.; El-kilani, R. M.; Nasr, G. E. M. Electrodeposition of Ni–ZnO nanocomposite for protecting the agricultural mower steel knives. *Chem. Pap.* **2021,** *75,* 139–152. https://doi.org/10.1007/s11696-020-01291-2

(64) Chen, W.; Gao, W. Sol-enhanced electroplating of nanostructured Ni–TiO_2 composite coatings: The effects of sol concentration on the mechanical and corrosion properties. *Electrochim. Acta* **2010,** *55,* 6865–6871. https://doi.org/10.1016/j.electacta.2010.05.079

(65) Naik, S. N.; Walley, S. M. The Hall–Petch and inverse Hall–Petch relations and the hardness of nanocrystalline metals. *J. Mater. Sci.* **2020,** *55,* 2661–2681. https://doi.org/10.1007/s10853-019-04160-w

(66) Arzt, E.; Dehm, G.; Gumbsch, P.; Kraft, O.; Weiss, D. Interface controlled plasticity in metals: Dispersion hardening and thin film deformation. *Prog. Mater. Sci.* **2001,** *46,* 283–307. https://doi.org/10.1016/S0079-6425(00)00016-9

(67) Hansen, N. Hall–Petch relation and boundary strengthening. *Scr. Mater.* **2004,** *51,* 801–806. https://doi.org/10.1016/j.scriptamat.2004.06.002

(68) Liu, W. H.; Wu, Y.; He, J. Y.; Nie, T. G.; Lu, Z. P. Grain growth and the Hall–Petch relationship in a high-entropy FeCrNiCoMn alloy. *Scr. Mater.* **2013,** *68,* 526–529. https://doi.org/10.1016/j.scriptamat.2012.12.002

(69) Xijing, L.; Yong, C. Effect of SiO_2 nanoparticles on the hardness and corrosion resistance of NiW/SiO_2 nanocomposite coating prepared by electrodeposition. *Int. J. Electrochem. Sci.* **2023,** *18,* 100138. https://doi.org/10.1016/J.IJOES.2023.100138

Draft

© The Author(s) or their Institution(s)

(70) Ma, C.; Wang, S. C.; Wood, R. J. K.; Zekonyte, J.; Luo, Q.; Walsh, F. C. Hardness of porous nanocrystalline Co–Ni electrodeposits. *Met. Mater. Int.* **2013,** *19,* 1187–1192. https://doi.org/10.1007/s12540-013-6006-y

(71) Meyers, M. A.; Mishra, A.; Benson, D. J. Mechanical properties of nanocrystalline materials. *Prog. Mater. Sci.* **2006,** *51,* 427–556. https://doi.org/10.1016/j.pmatsci.2005.08.003

(72) Broitman, E. Indentation hardness measurements at macro-, micro-, and nanoscale: A critical overview. *Tribol. Lett.* **2017,** *65,* 23. https://doi.org/10.1007/s11249-016-0805-5

(73) Saini, H.; Khatri, M. S. A tropical review on electrodeposition metal matrix nanocomposite coatings. *J. Electron. Mater*. **2025**, *54*, 6069–6095. https://doi.org/10.1007/s11664-025-12037-9

(74) Taheri, S. H.; Khazaei, B. A.; Rashidi, A. M.; Boroujerdnia, M.; Jamali-Sheini, F. Effect of codeposition of TiO_2 and SiC nanoparticles on microhardness, wear, and corrosion behavior of electrodeposited Ni–W-based nanocomposite coating. *Mater. Chem. Phys.* **2025,** *345*, 131183. https://doi.org/10.1016/j.matchemphys.2025.131183

Draft

© The Author(s) or their Institution(s)